Received: 6 May 2024 | Revised: 4 July 2024 | Accepted: 26 July 2024

DOI: 10.1002/cyto.a.24893

ORIGINAL ARTICLE

MIFlowCyt

ISAC INTERNATIONAL SOCIETY FOR ADVANCEMENT OF CYTOMETRY

CYTOMETRY Journal of Quantitative Cell Science PART A

High-throughput screen to identify and optimize NOT gate receptors for cell therapy

S. Martire[1] | X. Wang[1] | M. McElvain[1] | V. Suryawanshi[1] | T. Gill[1] | B. DiAndreth[1] | W. Lee[1] | T. P. Riley[1] | H. Xu[2] | C. Netirojjanakul[1] | A. Kamb[1]

[1]A2 Biotherapeutics, Agoura Hills, California, USA

[2]Port Therapeutics, Los Angeles, California, USA

Correspondence
S. Martire and A. Kamb, A2 Biotherapeutics, 30301 Agoura Road, Agoura Hills, CA 91301, USA.
Email: smartire@a2biotherapeutics.com and akamb@a2biotherapeutics.com

Abstract

Logic-gated engineered cells are an emerging therapeutic modality that can take advantage of molecular profiles to focus medical interventions on specific tissues in the body. However, the increased complexity of these engineered systems may pose a challenge for prediction and optimization of their behavior. Here we describe the design and testing of a flow cytometry-based screening system to rapidly select functional inhibitory receptors from a pooled library of candidate constructs. In proof-of-concept experiments, this approach identifies inhibitory receptors that can operate as NOT gates when paired with activating receptors. The method may be used to generate large datasets to train machine learning models to better predict and optimize the function of logic-gated cell therapeutics.

KEYWORDS
FACS, function-based screen, ITIM, logic gate, NOT gate, Tmod

1 | INTRODUCTION

As the opportunity to exploit novel single antigens for cancer passes, drug discovery has focused more on multi-antigen profiles to discriminate between tumor and normal cells [1]. Cell therapy is an ideal modality for this purpose because cells naturally integrate complex information to formulate an output; for example, to proliferate and kill target cells [2]. In the field of synthetic biology, engineered cellular systems of this type are often referred to as logic gates [3]. One type of logic gate, the NOT gate, responds to two inputs: the presence of antigen A and absence of antigen B. Perhaps the best studied NOT gate is called Tmod, which consists of an activator (e.g., a chimeric antigen receptor, CAR) that is coexpressed with an inhibitory receptor, or blocker. Together the two receptors control cell cytotoxicity, proliferation, and cytokine release [4]. Though other inhibitory receptors can function as NOT gates, Tmod utilizes an inhibitory receptor based on the LILRB1 gene product that contains 4 ITIM sequences [5]. Most Tmod constructs target HLA gene products with the blocker scFv [6–9], although Tmod is also capable of accommodating a wide variety of blocker antigens [10].

Much progress has been made toward understanding the properties of Tmod [10–12]. However, the system is considerably more complicated than conventional therapeutics; it involves two antigens and two receptors compounded by the dynamics between the target and effector cells. This complexity poses challenges to understand the effect of receptor design on Tmod function. Computational models that use neural networks to predict structure–function relationships are improving, but the most effective models require large amounts of high-quality and well-labeled data [13].

Somatic cell genetics that involves screens of libraries of DNA constructs offers a potential solution [14]. One time-honored screening approach utilizes a fluorescence-activated cell sorter (FACS) combined with fluorescent reporters to select cells that contain genes of interest [15]. If the signal-to-noise characteristics of the assay are

sufficient, rare variants can be selected in an iterative process of enrichment [16].

Here, we present a FACS-based screen designed to identify blockers that function in the context of Tmod. Quantitative validation of the method in proof-of-concept enrichment experiments of inhibitory domains shows that it possesses features consistent with application to high-throughput screens. These future applications may include acquisition of large-scale data sufficient to train neural network models, bypassing the empirical process of experimental Tmod optimization.

2 | RESULTS

2.1 | Flow schema of function-based assay

The screening strategy centers on selection of variants from a library of receptors and is similar to approaches used by others to identify CAR variants [17]. The key difference in our approach is the increased complexity of a system that has two components with opposite effects, one activating and the other inhibitory. This difference requires additional steps in the enrichment process. Although the system could be utilized to screen for both components, we focused on the blocker as the differentiating and more uncharacterized element of the NOT gate.

The flow schema for screening includes a series of steps, beginning with library construction (Figure 1). A library of blocker variants is introduced into a lentiviral vector and transduced into Jurkat cells that express green-fluorescent protein (GFP) controlled by an NFAT-regulated response element. Although primary T cells can also be used (see Section 3), Jurkat cell lines are technically more feasible and predict most of the acute behavior of Tmod receptors [18]. The properties of the reporter line are critical and it is described in detail in the next section. Next, HeLa cells that express either the activator antigen (A cells) or both the A antigen and blocker antigen (AB cells) provide the activation and blocking stimuli, respectively. The target cells are cocultured with the Jurkat cells in two stages: (i) the Jurkat cells are activated by the A cells, and the reporter-positive fraction is collected via FACS; this step depletes constructs that contain inactive activators or blockers that are constitutively active (i.e., block independent of the blocker antigen); (ii) the resultant Jurkat cell population is exposed to AB cells and sorted to separate reporter-negative cells from reporter-positive cells that lack strong blocker function. After multiple iterations of this two-stage selection cycle, the enriched library of constructs is recovered from Jurkat cells by PCR and subjected to next-generation sequencing (NGS). Read counts of the various constructs allow estimates of the enrichment and, therefore, the relative functional activity of the blocker variants in the library.

2.2 | Design and optimization of a Jurkat reporter cell line

To create a cell line fit for the purpose of enriching blockers by FACS, Jurkat cells that contain a fluorescent reporter were constructed and optimized. The activation-inducible reporter consisted of a GFP gene

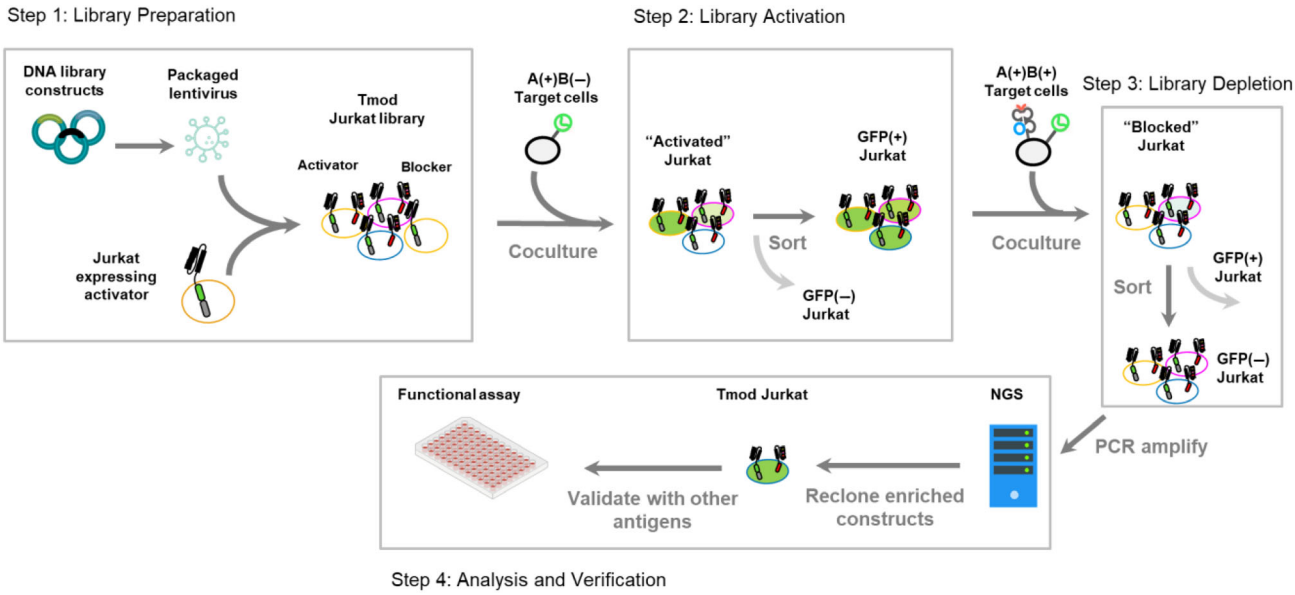

FIGURE 1 Flow schema of function-based assay. A library of blockers was cloned into a lentiviral vector and transduced into an optimized green-fluorescent protein (GFP)-reporter line of Jurkat cells that express a CAR activator. The Jurkat cell library was exposed to target cells expressing only the activator antigen (A(+)B(−)) and sorted using fluorescence-activated cell sorter (FACS) to isolate the activated GFP(+) population. Next, the GFP(+) Jurkat cells were exposed to target cells expressing both activator and blocker antigens (A(+)B(+)) and sorted to isolate GFP(−) fraction. FInally, the collected cells are analyzed by next-generation sequencing (NGS) to identify candidate blocker sequences enriched during the process.

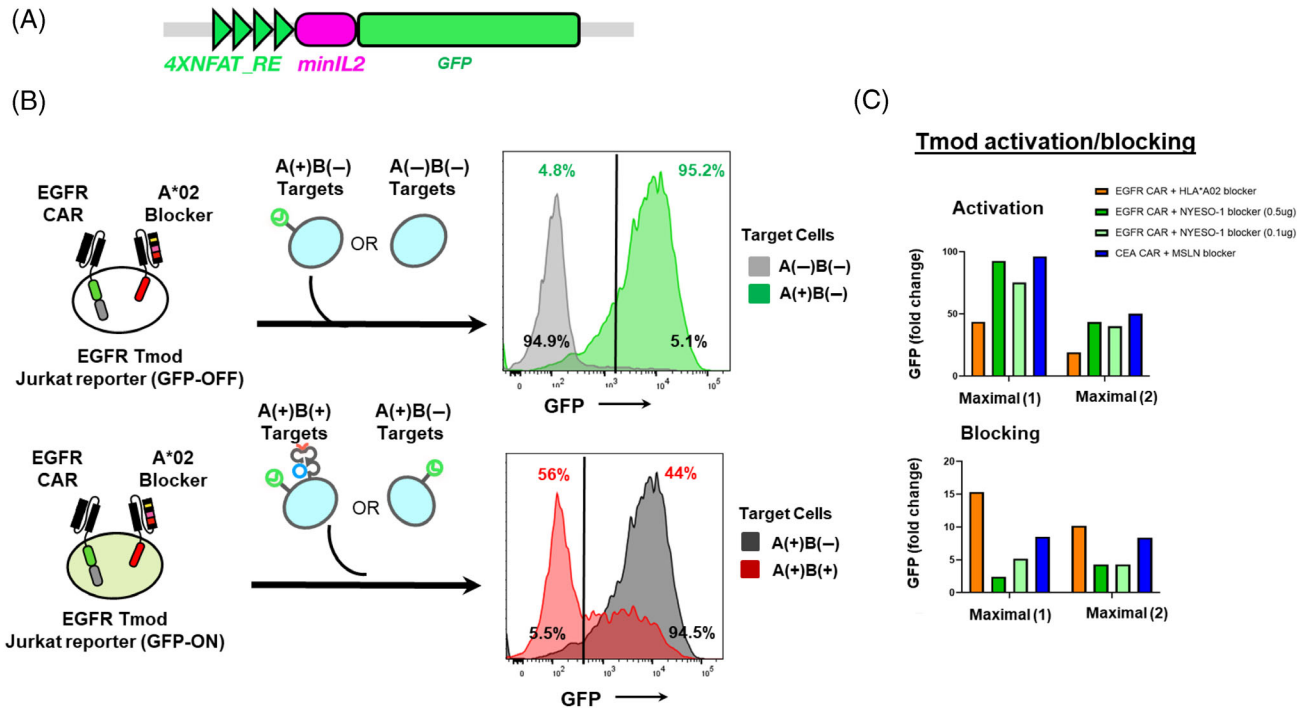

FIGURE 2 Engineering and validation of the Jurkat reporter cell line. (A) Jurkat cells were transfected with a green-fluorescent protein (GFP) gene downstream of an NFAT/IL2 promoter. Clones were grown from limiting dilution and screened for low background and induction of GFP. (B) Validation of Jurkat reporter cell line. See Figure S1A for optimization of coculture conditions. Activation (top): HeLa cells that express A antigen (EGFR) were presented to the Jurkat reporter cell lines (transduced with EGFR CAR), to activate the NFAT promoter and GFP signal. Maximal activator enrichment was calculated as %GFP(+) in the activated population to the right of the gate divided by %GFP(+) of the uninduced population to the right of the gate. Blocking (bottom): Next, Jurkat cells that expressed both the EGFR CAR and an HLA-A*02 blocker were cocultured with HeLa cells that express both target antigens (A(+)B(+)). Maximal blocker enrichment was calculated as %GFP(−) in the blocked population divided by %GFP(−) in the unblocked population. (C) Maximal enrichments for three Tmod activator/blocker pairs (EGFR/HLA-A*02, EGFR/NY-ESO-1 (at two blocker target levels), and CEA/MSLN) was measured as described above. 1 = Maximal enrichment when gates are placed at peaks of each distribution as in Figure S2; 2 = Maximal enrichment when peaks are placed at the trough between peaks (Figure S1B). GFP fold-change refers to the fraction of cells in a gate defined by a GFP threshold.

located downstream of an NFAT-regulated promoter (Figure 2A). After introduction into Jurkat cells via electroporation (see Section 4), individual clones were screened by FACS. A clone was identified that maintained low background expression of GFP in the absence of a stimulus, and strong GFP induction by the general T cell activation cocktail ionomycin/phorbol/12-myristate 13-acetate.

The selected Jurkat reporter clone was further characterized quantitatively by measuring its activation and blocking windows by flow cytometry (Figure 2B). For this purpose, an EGFR-specific CAR (see Section 4) was introduced by lentivirus transduction. Jurkat cells were cocultured with HeLa target cells at an effector: target ratio (E:T) of 1:1, and GFP fluorescence was measured after 18 h (Figure S1A). The maximal activation window, defined as the percentage of GFP(+) cells cocultured with A(+) cells divided by the percentage cocultured with A(−)B(−) cells was ∼20 fold (Figure 2B,C). To benchmark the blocking window, an HLA-A*02 blocker with known function (see Section 4) was introduced into the EGFR CAR-containing Jurkat cells by lentivirus. The maximal blocking window, defined as the fraction of GFP(−) cells cocultured with A(+)B(+) target cells divided by the fraction of GFP(−) cells cocultured with A(+)B(−) cells, was ∼10× (Figures 2B,C and Figure S1B). A second blocker directed at the NY-ESO peptide presented by HLA-A*02 (encoded by a tripartite construct consisting of the NY-ESO-$1_{157\text{-}165}$ peptide fused to HLA-A*02 and B2M) (Figure S1C–E; [19]) (referred to subsequently as NY-ESO-1) was also tested with the EGFR CAR. This Tmod receptor pair displayed similar activation but somewhat weaker blocking compared to the EGFR/HLA-A*02 Tmod construct.

To confirm that the induction properties of the Jurkat reporter cell line were not limited to the EGFR Tmod constructs, a second Tmod construct with a CEA activator and MSLN blocker were used. The activation windows were 90×, and the blocking windows >8× with the constructs (Figures 2C and S1E). To further buttress the comparison and solidify the timing of the coculture, the activation and blocking time-courses were tracked with a kinetic imaging assay (Figure S1F; see Section 4). The change in GFP level reached about half of its maximal value in ∼20 h, and within 40–48 h was nearly maximal for both activation and blocking. These data were confirmed by flow cytometry-based readout (Figure S1G,H) which showed maximal value at 18 h. Together, these results suggested that the Jurkat screening system for Tmod blockers was robust across multiple

constructs and enrichment of 2–15× was theoretically possible, depending on the characteristics of the specific Tmod construct and where the FACS selection gates were set [16].

2.3 | Selection of inhibitory intracellular domains from a library

With the development of a robust reporter cell line, we set out to test the system with a library of blocker variants. To this end, we created 46 variants of the NY-ESO-1 blocker described above, each with a different transmembrane domain and intracellular domain (TICD) fused to a LILRB1 backbone (Figure 3A, Table S5). Of the 46 blocker constructs, 34 encoded domains from proteins that are expressed in immune cells and thought to downregulate the immune response. Ten variants altered the LILRB1 intracellular domain, and two were null variants, one with all ITIM domains removed and the other with mutations in all ITIM domains. The 10 LILRB1 variants included different subvariants of the 4 ITIM sequences from LILRB1 with combinations of point mutations that alter the conserved tyrosine phosphorylation site in the ITIMs (Figure 3B; [20]). One of the presumptive non-functional ICDs had point mutations removing the tyrosine in each of the 4 ITIMs; the other presumptive non-functional construct encoded a truncated ICD with no ITIM sequences. These blocker constructs were tested in two separate enrichment studies using two independent activators directed at EGFR; a strong EGFR activator and a weak EGFR activator (Section 4).

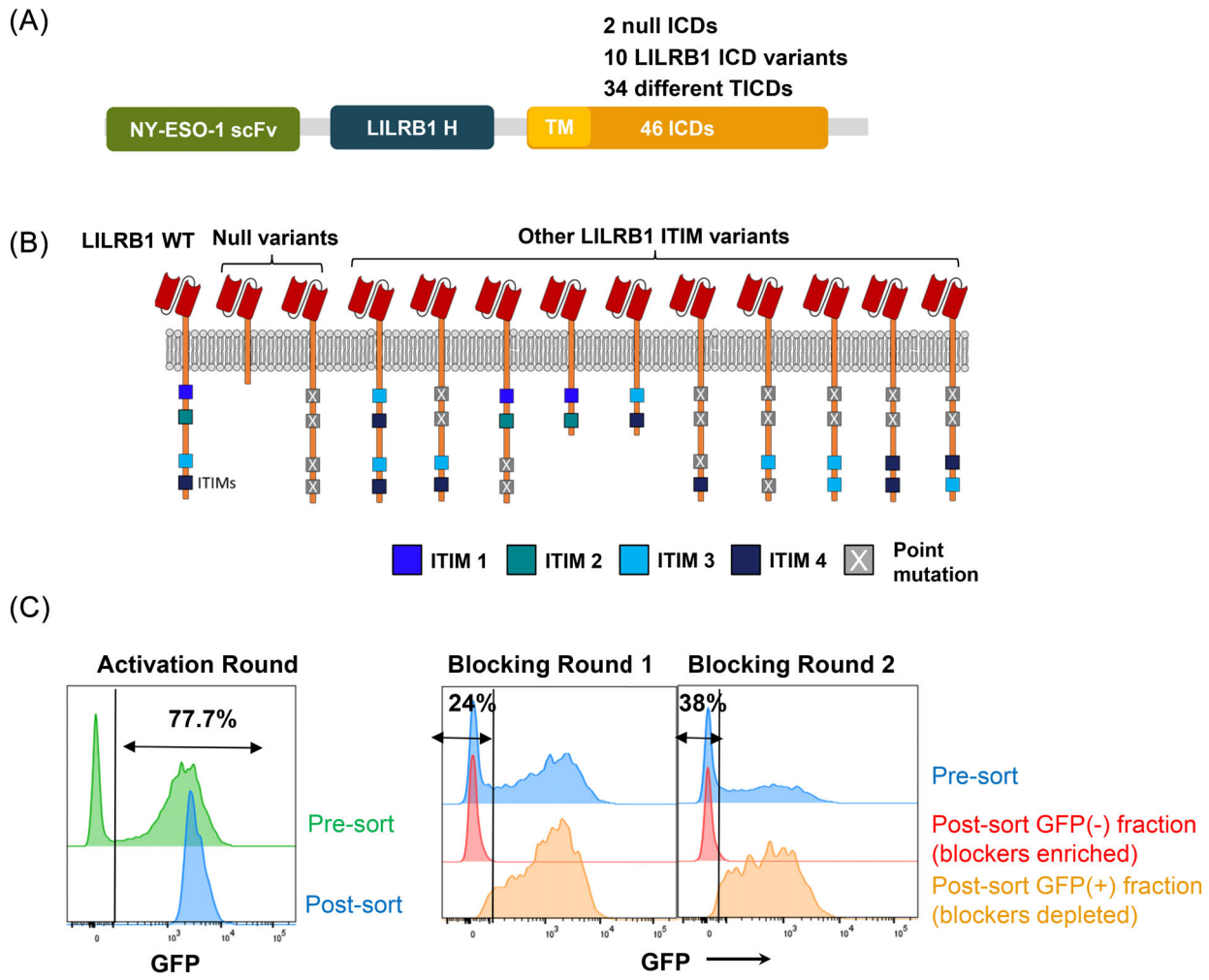

FIGURE 3 NY-ESO-1 blocker library construction and screening. (A) The blocker library comprised 46 constructs with NY-ESO-1 scFv, LILRB1 hinge (H), transmembrane domains (TM), and 46 different intracellular domains (ICDs) (2 null ICDs, 10 LILRB1 ICD variants, and 34 different TICDs). (B) LILRB1 wild-type (WT) and null variants of the ICD domains were chosen as positive and negative controls. ICDs with a variety of shuffled and mutant LILRB1 ITAMs were included in the library. (C) Jurkat reporter cells that express the strong EGFR CAR and blocker library were cocutlured with A(+) HeLa cells that express EGFR, sorted for the green-fluorescent protein (GFP) (+) population to enrich for cells able to activate. After recovery in media, activated cells were cocultured with A(+)B(+) HeLa cells that express EGFR and NY-ESO-1 trimer and sorted for GFP(+) and GFP(−) fractions. Flow plots show the gates for the activation step and the first blocking round. See Figure S3 for additional information on the construct, list of ICDs, and enrichment and for flow plots derived from enrichment of the weak EGFR CAR library.

The individual blocker constructs were cloned and pooled into a single library, packaged into lentivirus (see Section 4), and transduced into the Jurkat reporter line stably expressing one of the EGFR CARs (either strong or weak CAR) at a multiplicity of infection (MOI) of 0.5. The resulting population of Jurkat cells that expressed both activator and blocker was enriched to near purity (100% Tmod(+) cells) (Figure S2A). A reactivation experiment confirmed that the Tmod-enriched cells could be reactivated by A(+)B(−) cells (Figure S2A).

The pure Tmod(+) Jurkat cells that expressed the strong EGFR CAR and the library of blocker variants were exposed first to A cells and sorted to isolate GFP(+) Jurkat cells as described above. Around 80% were in the GFP(+) gate, confirming previous data (Figures 2B and 3C). After recovery in media, these GFP(+) cells were cocultured with AB target cells that expressed both EGFR and an NY-ESO-1-HLA-A*02 trimer (see Section 4). Roughly 24% of cells were in the GFP(−) gate (Figure 3C). After one cycle of exposure to AB cells, the sorted GFP(−) cells were grown for 7 days and exposed for a second time to AB cells, this time with 10× lower A antigen (NY-ESO-1) and the GFP(−) and GFP(+) subpopulations were collected for analysis. Similar steps were repeated for the blocker library in Jurkat cells that contained the weak EGFR CAR (Figure S2B).

2.4 | Results and confirmation of selected inhibitory receptor constructs

To identify enriched blocker constructs, the various pre- and post-sort Jurkat cell fractions were subjected to NGS using the PacBio Sequel system to generate read lengths that encompassed the TICD variants lengths that are >500 bp (Figure 4A; see Section 4). These TICD sequence reads from both weak and strong activator screens were mapped to the library sequences, allowing comparison of the counts and frequencies of each variant (Figures S3A and 4A; Table S7). More than 90% of the reads were aligned successfully to the library sequences, with an average read number per variant of 5000, depending on the fraction (Figure 4A). Frequencies of the 46 constructs in the input library were roughly equal. Only one construct (G6B) had *z*-score >3.

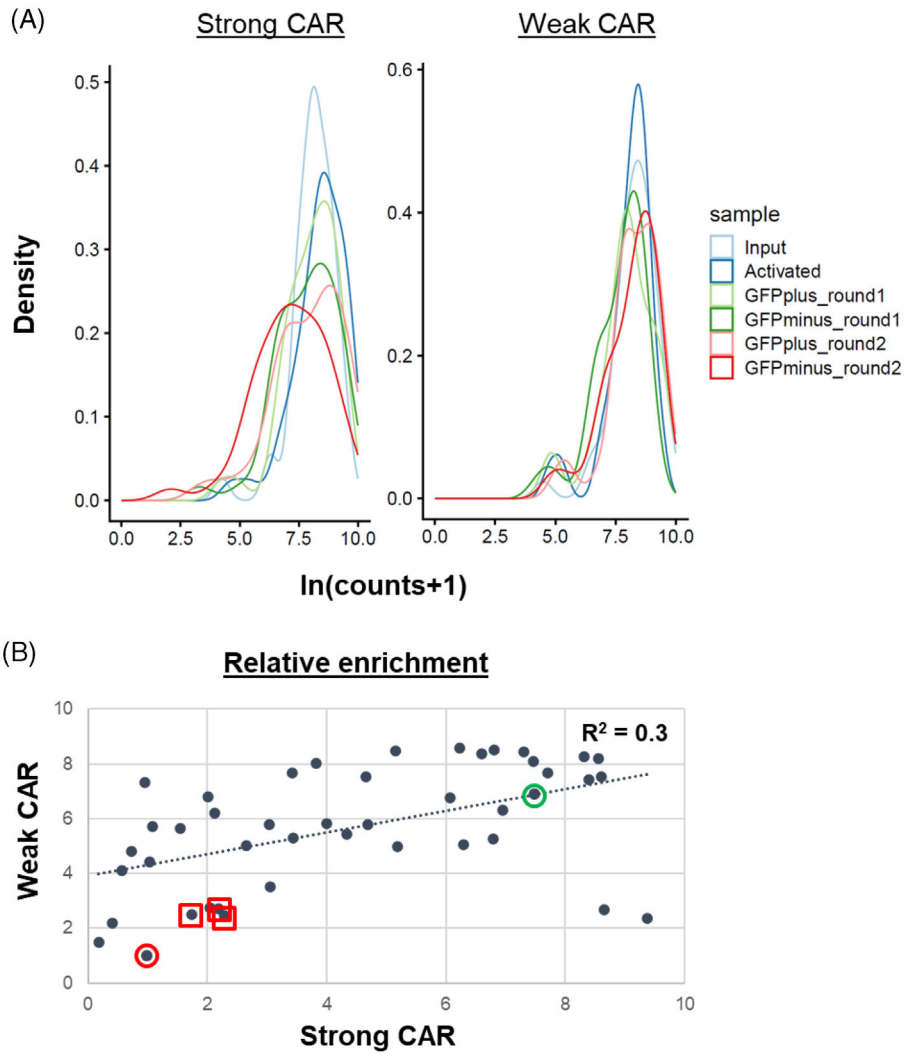

FIGURE 4 Enrichment analysis by next-generation sequencing (NGS). (A) Density plots of alignment of samples derived from various subpopulations of cells pre- and post-sorting. >90% of reads were successfully aligned to the reference library. (B) Scatter plot of enrichment values for strong and weak EGFR CAR experiments. Enrichment is calculated as the ratio of variant frequencies in the round 2 sample divided by the frequency in the activated sample prior to round 1. This enrichment is divided by the negative control (LILRB1 with truncated ICD) to give enrichment relative to the negative control. In this plot, two outliers were removed. The LILRB1 WT positive control is circled in green. The negative control in red. The three variants with <2 WT ITIMs are boxed in red. See Table S6 for ranked list of library constructs from both strong- and weak-CAR experiments. Note that two outliers (>9 enrichment) in weak CAR library were excluded in the plot.

An enrichment score relative to the negative control (the LILRB1 null variant with truncated ICD removing all ITIM domains), measuring the abundance of blocker variants in the output versus the activated input samples (see Figure 1), was computed for each construct in both experiments (Figure 4B). The activated input samples were used to calculate the enrichment score given the high similarity observed between input and activated samples (Figure S3B). The results showed a frequency increase of the positive control (LILRB1) compared to the negative control, suggesting that the method effectively enriched functional blockers. For both the strong and weak EGFR CAR experiments, the LILRB1 wild-type sequence was enriched ~8× compared to the input activated fraction (Figure 4B, Table S6). The second enrichment cycle, conducted at 10× lower blocker antigen levels, produced little effect, suggesting the antigen level might fall below the threshold for detectable blocker activity under the conditions of the selection.

With regard to rank order of enrichment, in the strong-CAR experiment the positive control ranked 9th of the 46 constructs; only one higher-ranking construct (EPOR) was enriched more than 2× relative to the positive control and it was later proven to express poorly on the surface, potentially enriching due to a ligand-independent effect. The negative control ranked 41 out of 46. In the weak CAR experiment, the positive control was 11/46 and the negative control 46/46. These results suggested that the weak CAR provided a more sensitive system to select blockers. Nonetheless, there was reasonable correlation between the two enrichment datasets, with only a few outliers (Figure 4B). Interestingly, of the LILRB1 variants, only the variants with at least two wild-type ITIMs showed consistent enrichment for blocker function. Those with only one or no ITIMs were within 2× of the negative control.

To validate the enrichment results further, a subset of the enriched variants were analyzed in Jurkat cells as individual blockers with five different activators (Figure 5A, Figure S4A,B). Activation in these Jurkat cells, the parental line used to generate the GFP reporter line described above, was measured using an NFAT-luciferase reporter [20,21]. These studies confirmed that all the top enriched constructs functioned as Tmod blockers, and furthermore, that LILRB1 was the most powerful blocker of the set, based on the average percent blocking observed for all the Tmod constructs (Figure 5B,C). In a separate experiment, we used NFAT-luciferase Jurkat cells transiently transfected with MAGE-A3 CAR and NY-ESO-1 blocker to test blocker strengths in constructs comprising the 34 ICDs and LILRB1. The data from this assay roughly correlated with the enrichment of these blocker constructs, especially when compared

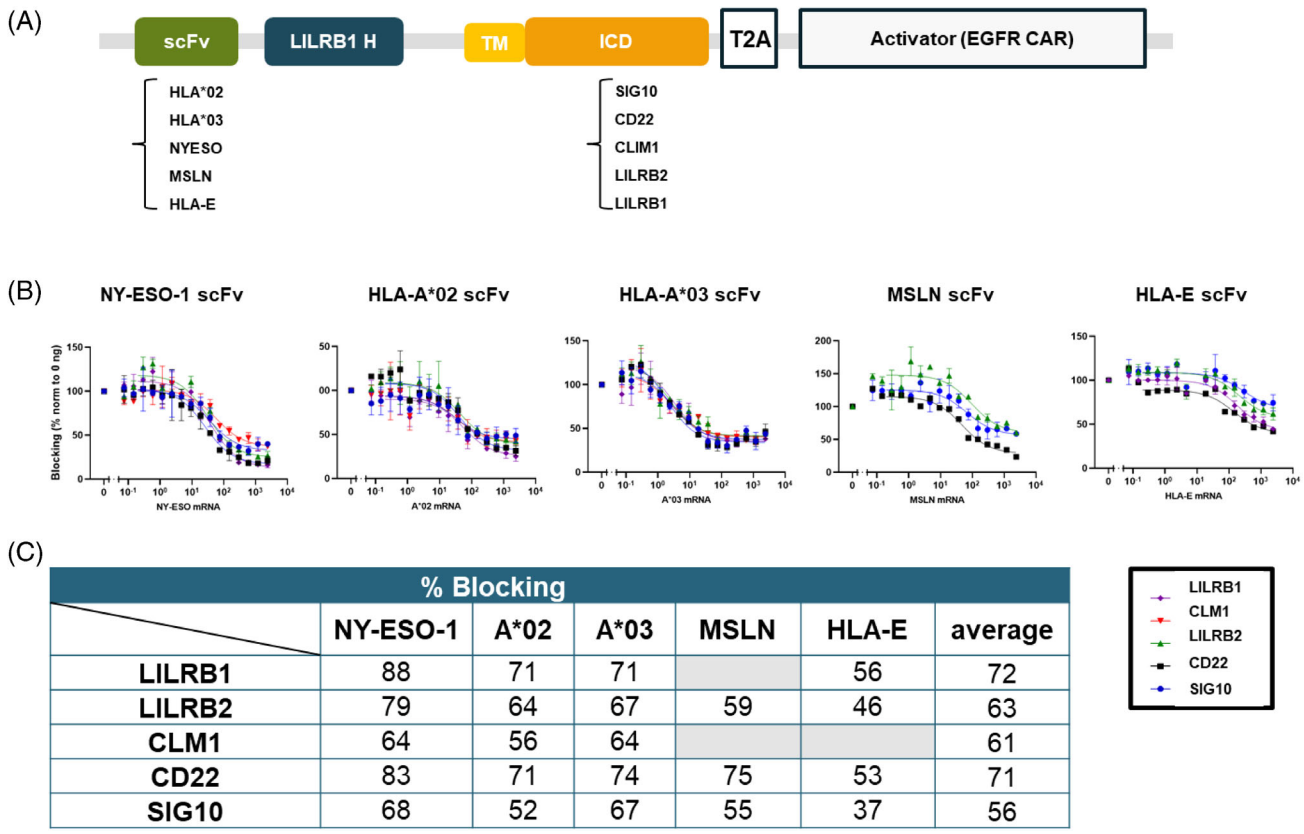

(C)

% Blocking	NY-ESO-1	A*02	A*03	MSLN	HLA-E	average
LILRB1	88	71	71		56	72
LILRB2	79	64	67	59	46	63
CLM1	64	56	64			61
CD22	83	71	74	75	53	71
SIG10	68	52	67	55	37	56

FIGURE 5 Functional assay to confirm blocking of enriched ICDs using five blockers. (A) Diagram of the five blocker constructs that were chosen and cloned into a single vector containing five different scFvs and the EGFR CAR. Activator and blocker are encoded by a single polypeptide separated by a T2A cleavage site. (B) Functional assays in Jurkat NFAT-luciferase reporter cells using HeLa target cells that express the different activator antigens, titrated with blocker antigen mRNA (see Section 4). The plots show comparable dose-dependent blocking of all the constructs tested. (C) Percent blocking of five activators with selected enriched blocker constructs, including positive control (LILRB1).

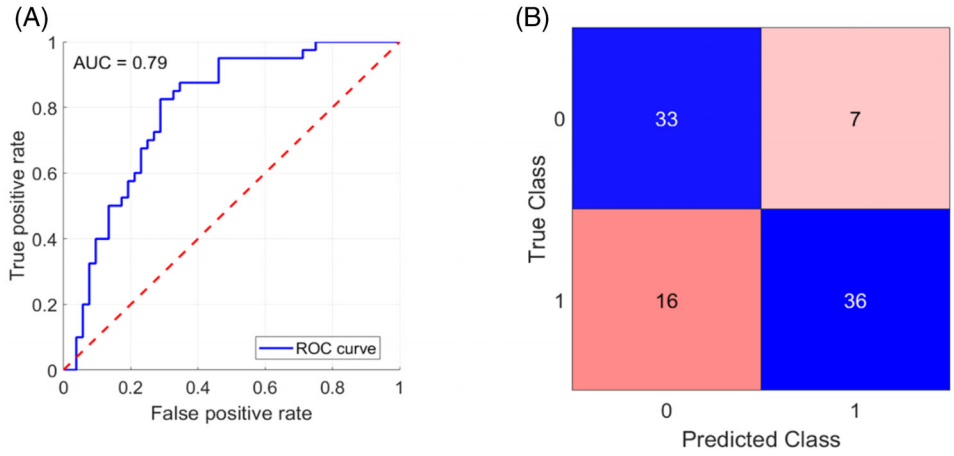

FIGURE 6 Machine learning models identify predictors of enrichment. (A) Area under the curve (AUC) of the receiver operating characteristic (ROC, blue line) quantifies the predictive power of a machine learning model trained to predict final enrichment of the Tmod constructs. AUC = 1—perfect prediction; AUC = 0.5—no predictive power; AUC = 0—inverted prediction. (B) Confusion matrix of the same model quantifies and compares the correct predictions (true negative and true positive; blue) with the incorrect predictions (false positives and false negatives [red]).

with the weak EGFR CAR (Figure S5). Together with the enrichment rank order, these functional validation results suggested that the system developed here is a reliable screening platform for selection of blocker variants by FACS.

2.5 | Identifying significant predictors of blocker enrichment

To further characterize the data from the enrichment results, we constructed several linear regression and machine learning models to identify predictors of enrichment. Although only 92 input values were used, the enrichment data enabled some simplistic feature selection. Briefly, we incorporated 8 preselected features (Table S8) into different models design to predict either a successful or unsuccessful enrichment event. After a nested 5-fold cross validation [22], most models successfully predicted the blocker behavior with 70%–80% accuracy (Figure 6), suggesting that the selected features are indeed predictors of Tmod function. Although interpreting the weights of inputs used within a neural network is difficult due to the complexity and nonlinear nature of the models, the weights of the model suggested that CAR strength, ITIM count, and total number of tyrosines were the most significant predictors of function.

3 | DISCUSSION

We adapted a traditional method of variant selection in somatic cells that combines an optimized reporter line with FACS to enrich inhibitory receptors that comprise part of a dual-receptor NOT gate. The final workflow from library design to data analysis required ~3 months. A proof-of-concept study using a blocker library of 46 variants, including structural variants of the LILRB1 ICD and TICDs from 34 other presumptive inhibitory receptors, demonstrated enrichment of specific functional constructs, confirmed via subsequent in vitro studies. The method is general and robust; it works with activators of different strengths and yields blocker variants that function with multiple blocker antigens.

The use of pooled libraries and FACS selection enables high-throughput evaluation and optimization, but some compromises restrict broad applicability. In addition to technical limitations (cell death during FACS, PCR-biased amplification, NGS depth, cell growth rates, etc.), the selections must be sufficiently robust with regard to signal to withstand certain types of noise; in particular, variable penetrance and expressivity of the genetic variants in the library [16]. Although the results suggest that activator and blocker function controls Jurkat cells in a binary, rather than a graded fashion based on the clear bimodal distribution of GFP in the induced and blocked populations (Figure S1G,H), the kinetics of reporter induction and turnover likely introduce some variability that limits enrichment. In addition, although libraries can be screened at low MOI, Poisson statistics determine that some passenger constructs co-segregate with the functional constructs, again limiting the enrichment observed. These and other sources of noise should be mitigated by further rounds of enrichment. Ultimately the main determinant of the enrichment is the signal-to-noise behavior of the reporter line, justifying substantial investment up-front in its optimization. In the case described here, the Jurkat reporter line displayed an ~50× induction ratio and an ~10× inhibition ratio, the maximal limit of enrichment per cycle.

Other approaches have been used to screen for, or select, receptors with improved function; for example, high-throughput methods that involve plate-based analysis of isolated constructs or small pools [23]. In addition, alternative platforms can substitute for the flow cytometer [24]. However, these approaches are more limited than flow cytometry with regard to throughput; however, they can have superior signal-to-noise properties because of the analysis of

single constructs. Such high-throughput methods have been used to empirically identify CAR components that include signaling [25,26] and ligand-binding domains [17]. However, FACS-based methods have not been developed for Tmod and other NOT gates. Notably, the method described here uses Jurkat cells to model T cells, a considerable technical simplification. Others have used primary T cells for FACS-based selections, an approach that may have certain benefits, but for selections based on acute effects, we believe that the convenience of Jurkat cells is worth the potential trade-off [27]. Furthermore, T cell viability is often compromised by multiple rounds of sorting.

In these experiments, several TICDs showed significant enrichment as blocker components. The LILRB1 ICD emerged as the strongest blocker, an observation consistent with previous reports [4]. These studies also demonstrate the value for structure–activity relationship (SAR) analysis. The ITIM sequences of LILRB1 were probed via point mutations of the conserved tyrosine residues. Although the results did not have the power to definitively determine rank order, the observed trends were consistent with expectations that at least 2 ITIMs are required for effective inhibitory signaling. The ability to create large libraries with thousands of constructs, coupled with the FACS system described here, suggests a plausible approach to generate the input to train machine learning models. Indeed, the simplistic model developed here with limited data suggests such a system could provide a powerful tool to predict optimal properties of logic gates based on sequence alone. This assay could also be used to screen receptors that target multiple different antigens as well as potency boosters which could improve the discrimination of tumor cells and the potency of logic gates, respectively.

4 | METHODS

4.1 | Materials

All cell lines used in this study are listed in Table S1. Lentiviruses were outsourced to Alstem and are listed in Table S2. Constructs were cloned into a backbone that contained pLenti-EF1a promoter. Packaged lentivirus constructs were provided as frozen VSV-G pseudotyped viral particles. The titer was defined by Clontech's Lenti-X qRT-PCR Titration Kit (Cat. # 631235) and was typically >1 × 10^8 IFU/mL. Antibodies and recombinant proteins are listed in Table S3. sgRNAs and primers sequences are listed in Table S4.

scFvs were designed using a flexible (G4S)3-GG linker to connect the VH and VL domains. All third-generation activator CAR constructs contained the CD8a hinge fused to CD28 TM, as well as CD28, 4-1BB, and CD3z ICD. All blocker receptor constructs contained the LILRB1 hinge fused to the LILRB1 TM and ICD. All DNA constructs were assembled using Golden Gate Assembly and are listed in Table S5.

4.2 | Cell line generation

Unmodified cell lines were purchased from ATCC and grown per vendor instructions. To generate the Jurkat reporter cells, an optimized NFAT/IL-2 reporter that generates a GFP output was transduced, single-cell-sorted and screened for high-functioning clones. The Jurkat reporter cell lines were transduced with lentivirus of interest (CAR or blocker constructs; Table S2) at MOI 10 to make stable reporter cell lines.

HeLa cells were used as target cells and they were engineered depending on the Tmod pair used. Wild-type HeLa cells were transduced with RFP/Fluc (red fluorescent protein/firefly luciferase) using lentiviral vectors (Biosettia) to discriminate HeLa from Jurkat cells during cell sorting. Since HeLa cells do not express CEA, they were subsequently transfected with an expression vector (Table S5) harboring the CEACAM5 sequence and G418 selection marker. EGFR(−) or MSLN(−) HeLa were generated by CRISPR-KO: RNP complexes were formed by mixing S.p. HiFi Cas9 protein (Integrated DNA Technologies) and sgRNAs at 1:3 molar ratios before electroporation using the 4D Nucleofector (Lonza). Guide RNAs were purchased from Synthego or IDT (Table S4). The target knockout or over-expressing cell lines were enriched for target-negative or -positive pools, respectively, by FACS using appropriate antibodies. To generate transient NY-ESO-1 (+) or MSLN(+) cells and other blocker targets, Hela cells expressing EGFR or CEA (target A) cells, were transfected with mRNA using a 4D Nucleofector, and assays were performed within 1–3 days post transfection (see below).

4.3 | In vitro transcription of mRNAs

The standard in vitro transcription reaction of mRNAs was carried out in a 25 µl of 1× reaction buffer containing 40 mM Tris–HCL, 10 mM dithiothreitol, 2 mM spermidine, 0.002% Triton X-100, 27 mM magnesium acetate, 5 mM CleanCap Cap 1 AG trimer (TriLink), and 5 mM each of ATP, CTP, GTP, and pseudouridine triphosphate (NEB). The reaction was incubated for 2 h at 37 °C with final concentrations of 8 U/µL T7 RNA polymerase (NEB, M0460T), 0.002 U/µL inorganic pyrophosphatase (NEB, M2403L), 1 U/µL murine RNase inhibitor (NEB, M0314L), and 0.025 µg/µL linearized-T7-template. A final 0.4 U/µL DNase I (NEB, M0303L) digestion was done at 37 °C for 15 min in 1× DNase I buffer to remove template. A standard poly(A) tailing step of RNAs was performed according to manufacturer's protocols with E. coli poly(A) polymerase (NEB, M0276), and RNAs were purified by a supplier's cleanup kit (NEB, T2040L). Purified RNAs were treated with 0.2 U/µg Antarctic phosphatase (NEB, M0289L) in 1× Antarctic phosphatase buffer for 1 h and repurified (NEB, T2040L). RNA concentrations were measured by Nanodrop and examined on 1% Agarose gel.

4.4 | Flow cytometry

To evaluate surface expression of CARs, cells were stained with soluble EGFR-Fc or CEA-Fc followed by APC-labeled anti-human IgG Fc. Briefly, 0.25–0.5 µg/mL of protein was incubated for 40–60 min at RT (room temperature). Two additional washes with FACS buffer (PBS + 2% BSA), were then performed, followed by staining with

streptavidin-fluorophore (fluorophore = PE or APC, as indicated) at 0.1 mg/mL at room temperature for 30 min. Washed twice with FACS buffer, cells were analyzed via flow cytometry for CAR expression (based on % of APC or PE-positive staining compared to unstained UTD cells, as indicated). To evaluate surface expression of the blocker, cells were labeled with biotinylated-pMHC probes, generated as described previously [17], tetramerized and prelabeled with streptavidin conjugated to an appropriate fluorochrome. After staining at 4 °C, median fluorescence intensity (MFI) was determined using a FACS Canto II flow cytometer. To evaluate surface expression of proteins on target cells, transiently transfected cells were tested with primary antibody (Table S3). Briefly, after one wash with FACS buffer (PBS + 2% BSA), cells were stained with primary antibodies for 40–60 min at room temperature (1:100 dilution, according to the manufacturer's instructions). After one wash with FACS buffer cells were incubated with secondary antibody (anti-mouse IgG Alexa Fluor™ 647) for 40–60 min at room temperature (1:2000 dilution). After two additional washes with FACS buffer (including 1 μg/mL DAPI to stain dead cells), cells were analyzed via flow cytometry for target expression.

4.5 | Target cell mRNA transfection

On the day of transfection, target cells were counted, washed with 1× PBS and resuspended in SE transfection buffer (Lonza). Target antigen mRNA was diluted to specific concentrations, and mRNA/cell mixtures were transferred to a 16- or 384-well Lonza 4D cuvette and electroporated according to the manufacturer's protocol. Post transfection, the cells were placed into MEM growth media containing serum and seeded into rows of 384-well culture plates at a density of 10,000 cells/well. Remaining transfected cells were seeded into separate 96-well plates for expression testing by flow cytometry (BD Canto). Plates were cultured for >16 h at 37°C and 5% CO_2.

4.6 | FACS coculture assays

CAR-expressing cells were cocultured in a 1:1 ratio with target EGFR or CEA-expressing cells (HeLa WT, HeLa CEA+) or non EGFR or CEA-expressing cells (HeLa EGFR KO, HeLa WT) in RPMI medium for 18 h. Jurkat suspension cells were collected and washed in DPBS with EDTA 2 mM. GFP fluorescence was assessed using FACSAria (BD) to quantify activation. In a similar fashion, Tmod-expressing cells were cocultured in a 1:1 ratio with activator and blocker antigens expressing cells, and GFP fluorescence was assessed to quantify blocking. MFI,% activation, and % blocking was used to compare several conditions and optimize the best conditions for the assay.

Maximal activator enrichment was calculated from the flow data as %GFP(+) in the activated population to the right of the gate divided by %GFP(+) of the uninduced population to the right of the gate. Maximal blocker enrichment was calculated as %GFP(−) in the blocked population divided by %GFP(−) in the unblocked population.

4.7 | IXM assays

Similar to FACS coculture assay, target cells expressing activator and blocker antigens were cocultured with Jurkat and whole-well GFP signal was monitored over time on ImageXpress Micro Confocal imager (Molecule Device Corporation) with a 4× objective. Target cells were seeded in 384-well poly-d-lysine–coated plates (Greiner Bio-One) for cell imaging. The next day target cells and Jurkat cells were cocultured 1:1 for up to 72 h, and total fluorescence area or intensity was recorded over time. To measure activation, Jurkat cells were coculture with HeLa cells presenting antigen A (EGFR or CEA), and GFP signal was measured overtime. To measure blocking, Jurkat cells were first cocultured overnight with HeLa cells presenting antigen A, followed by coculture with HeLa presenting antigen A plus antigen B (HLA-A*02, NY-ESO-1, MSLN). GFP signal was measured overtime. Increase and reduction of fluorescence signal in Tmod cocultures compared to wells cocultured with WT Jurkat.

4.8 | Blocker functional selections

In preparation for selections, 1E7 Jurkat cells were transduced with lentivirus at an MOI of 0.5. Virus was removed after 24 h of transduction, and the cells were scaled up and enriched with anti-Fc protein, representing the input sample. For a round of activation, cells were incubated overnight with HeLa cells expressing EGFR (antigen A), then sorted on a BD FACS Aria II (with at least 5E5 cells being collected) for GFP(+) expression. Cells were then rested without antigen and expanded for 7 days before subsequent rounds of selection. For blocking, cells were incubated overnight with HeLa cells presenting EGFR and antigen B (1 μg/0.2E6 cells NY-ES-O-1), then sorted on a BD FACS Aria II (with at least 5E5 cells being collected) for GFP(−) expression. For the second round of blocking a reduced amount of antigen B was presented (100 ng /0.2E6 cells). After each round of selection, at least 1E6 cells were sampled for NGS sequencing (whereas 6E7 and 2E7 cells were sampled for unselected and EGFP-sorted groups, respectively).

4.9 | Jurkat cell functional assay

Individual expression constructs were made using blockers containing either of five different scFvs targeting NY-ESO-1, HLA-A*02, HLA-A*03, MSLN, or HLA-E, LILRB1 hinge, LILRB1 TM, and a subset of the enriched ICDs. These blocker constructs were fused to a single activator gene directed at EGFR, using an scFv derived from cetuximab. Target cells were electroporated using 4D Nucleofactor (Lonza) with variable amounts of NY-ESO-1, HLA-A*02, HLA-A*03, MSLN, and HLA-E mRNA, ranging from 2 μg to 0.03 ng of mRNA in a 2-fold dilution series. In addition, no-mRNA and media-only controls were included in the same assay. The electroporated cells were seeded and grown under normal tissue culture conditions at a density of 10,000 cells/well in a 384-well plate for 18–20 h. Tmod constructs

(3 ug/2E6 cells) were electroporated into Jurkat NFAT-luciferase reporter cells and plated in 24-well plates for 18–20 h. The day after the electroporation 10,000 Jurkat NFAT-luciferase reporter cells (BPS Bioscience), wild-type or expressing Tmod constructs, were added to the target cell wells and cocultured for 6 h before luciferin substrate was added and the luciferase signal measured using Tecan Infinite M1000. Percent inhibition was calculated as the ratio between luminescence from Jurkat cells co-cultured with target cells treated with the highest mRNA concentration of blocker target, and luminescence from Jurkat cells cocultured with target cells expressing no blocker target. For the MAGE-A3 CAR experiment, a MAGE-A3 peptide titration in the presence or absence of 10 μM NY-ESO-1 peptide was performed using T2 cells [11,18]. The AUC (area under the curve) was calculated by subtracting the RLU values in the presence of the NY-ESO-1 peptide from the RLU values in the absence of NY-ESO-1 peptide among the MAGE-A3 peptide titrations.

4.10 | PacBio library generation

Approximately 1-2E6 cells were collected at each step of the functional screen and snap frozen. RNA was purified with RNAeasy kit, following the SOP (Qiagen), then treated with Turbo DNAse for 2 h at 37 °C. cDNA was made using 500 ng of RNA with SuperScript™ IV First-Strand Synthesis System (Thermo); cDNA was used for PCR amplification. The TICDs were amplified with Q5 MMix hifi HotStart polymerase (primers are listed in Table S4) and PCR product was purified using SPRI-beads by following the manufacturer's protocol (Beckman, B23317). PacBio libraries were prepared from 10 ng DNA, amplified following the SMRTbell Library Construction protocol (PacBio® Barcoded Overhang Adapters for Multiplexing Amplicons). The quality of the libraries was assessed using a D1000 ScreenTape on a 2200 TapeStation (Agilent) and quantified using a Qubit dsDNA HS Assay Kit (ThermoFisher). Libraries with unique adaptor barcodes were multiplexed and the final purified product was sent for targeted NGS sequencing (HudsonAlpha Institute for Biotechnology).

4.11 | PacBio sequence data quality control, alignment, and data analysis

HiFi consensus reads were aligned to the 46 ICD reference sequences by minimap2.1 with parameters optimized for PacBio hifi sequences (using the preset map-hifi). Only the primary/best alignments were retained by using the Samtools flag (−F 0 × 900) to filter out all secondary and supplementary alignments. The filtered sequences were used for generating a read counts matrix and further downstream analyses. The counts for each construct were normalized to its library size (total read counts) to generate construct frequencies. Enrichment values were calculated based on the change in construct frequency as described in the figure legends.

4.12 | Feature extraction and model training

Enrichment ratio data was converted into a binary metric with values greater than the mean enrichment ratio from both strong and weak CARs assigned an "enriched" value, and values less than the mean value assigned a "non-enriched" value. For preliminary model building, eight features were incorporated which described different elements of each Tmod cell (CAR, ICD amino acid length, LIR1 derivative, ITIM count, ITSM count, Total Tyrosines in ICD, Amino acid distance from transmembrane to first Tyrosine, Amino acid distance from last tyrosine to ICD end). Models were trained in Matlab R2022a with the statistics and machine learning toolbox. Briefly, the dataset of 92 data points was randomly split into 5 subsets for 5-fold cross validation (training and test datasets). These subsets were used to train hundreds of distinct models with different model architectures. Performance of each model was evaluated by the accuracy of the validation sets, which were not directly used in training. Top models were evaluated for architecture design and parameter weighting to identify significant features.

AUTHOR CONTRIBUTIONS

S. Martire: Writing – original draft; methodology; validation; conceptualization; investigation; writing – review and editing; formal analysis; project administration; data curation; supervision; visualization. **X. Wang:** Conceptualization; methodology; visualization; investigation; supervision; resources. **M. McElvain:** Methodology; investigation. **V. Suryawanshi:** Software; investigation; formal analysis. **T. Gill:** Investigation; data curation; visualization. **B. DiAndreth:** Validation; formal analysis; data curation. **W. Lee:** Investigation. **T. P. Riley:** Writing – review and editing; Investigation; formal analysis. **H. Xu:** Conceptualization; funding acquisition; methodology; supervision; resources. **C. Netirojjanakul:** Supervision; resources; project administration; writing – review and editing. **A. Kamb:** Conceptualization; data curation; formal analysis; visualization; writing – original draft; methodology; supervision; resources; funding acquisition; writing – review and editing.

ACKNOWLEDGMENTS

We thank members of the discovery research group at A2 Biotherapeutics for helpful discussions; Amanda Mock for generation of NY-ESO-1 probes; Mark Daris and Casey Gahrs for design and creation of key DNA constructs; Aaron Winters and Agnes Hamburger for critical comments on this manuscript; and Chuck Li for automation support.

CONFLICT OF INTEREST STATEMENT

All authors are shareholders and current or former employees of A2 Biotherapeutics Inc.

DATA AVAILABILITY STATEMENT

Datasets are deposited in the Dryad repository with the following DOI: https://doi.org/10.5061/dryad.np5hqc02v.

ORCID

S. Martire https://orcid.org/0000-0002-1570-3476

REFERENCES

1. Zimmermann GR, Lehar J, Keith CT. Multi-target therapeutics: When the whole is greater than the sum of the parts. Drug Discov Today. 2007;12(1–2):34–42.
2. Kamb A, Go WY. Cancer T-cell therapy: building the foundation for a cure. F1000Res. 2020;9:1295.
3. Bressler EM, Adams S, Liu R, Colson YL, Wong WW, Grinstaff MW. Boolean logic in synthetic biology and biomaterials: Towards living materials in mammalian cell therapeutics. Clin Transl Med. 2023;13(7):e1244.
4. DiAndreth B, Hamburger AE, Xu H, Kamb A. The Tmod cellular logic gate as a solution for tumor-selective immunotherapy. Clin Immunol. 2022;241:109030.
5. Hamburger AE, DiAndreth B, Cui J, Daris ME, Munguia ML, Deshmukh K, et al. Engineered T cells directed at tumors with defined allelic loss. Mol Immunol. 2020;128:298–310.
6. Tokatlian T, Asuelime GE, Mock JY, DiAndreth B, Sharma S, Toledo Warshaviak D, et al. Mesothelin-specific CAR-T cell therapy that incorporates an HLA-gated safety mechanism selectively kills tumor cells. J Immunother Cancer. 2022;10(1):e003826.
7. Tokatlian T, Asuelime GE, Naradikian MS, Mock JY, Daris ME, Martin AD, et al. Chimeric antigen receptors directed at mutant KRAS exhibit an inverse relationship between functional potency and neoantigen selectivity. Cancer Res Commun. 2022;2(1):58–65.
8. Sandberg ML, Wang X, Martin AD, Nampe DP, Gabrelow GB, Li CZ, et al. A carcinoembryonic antigen-specific cell therapy selectively targets tumor cells with HLA loss of heterozygosity in vitro and in vivo. Sci Transl Med. 2022;14(634):eabm0306.
9. Oh J, Kirsh C, Hsin JP, Radecki KC, Zampieri A, Manry D, et al. NOT gated T cells that selectively target EGFR and other widely expressed tumor antigens. IScience. 2024;27(6):109913. https://doi.org/10.1016/j.isci.2024.109913
10. Partin AC, Bruno R, Shafaattalab S, Vander Mause E, Winters A, Daris M, et al. Geometric parameters that affect the behavior of logic-gated CAR T cells. Front Immunol. 2024;15:1304765.
11. Manry D, Bolanos K, DiAndreth B, Mock JY, Kamb A. Robust in vitro pharmacology of Tmod, a synthetic dual-signal integrator for cancer cell therapy. Front Immunol. 2022;13:826747.
12. Mock JY, Winters A, Riley TP, Bruno R, Naradikian MS, Sharma S, et al. HLA-A *02-gated safety switch for cancer therapy has exquisite specificity for its allelic target antigen. Mol Ther Oncolytics. 2022;27:157–66.
13. Senior AW, Evans R, Jumper J, Kirkpatrick J, Sifre L, Green T, et al. Improved protein structure prediction using potentials from deep learning. Nature. 2020;577(7792):706–10.
14. Wheatley W, Yoo S, Pierce M, Rebentisch M, Endo M, Peterson I, et al. Genetic selection for modulators of the MAP kinase and beta-catenin growth-control pathways in mammalian cells. Biochem Genet. 2002;40:359–78.
15. Littman DR, Thomas Y, Maddon PJ, Chess L, Axel R. The isolation and sequence of the gene encoding T8: A molecule defining functional classes of T lymphocytes. Cell. 1985;40(2):237–46.
16. Sandrock R, Karpilow J, Richards B, Maxfield A, Wang C, Risley R, et al. Enrichment during transdominant genetic experiments using a flow sorter. Cytometry. 2001;45(2):87–95.
17. Fierle JK, Abram-Saliba J, Atsaves V, Brioschi M, de Tiani M, Reichenbach P, et al. A cell-based phenotypic library selection and screening approach for the de novo discovery of novel functional chimeric antigen receptors. Sci Rep. 2022;12(1):1136.
18. Xu H, Hamburger AE, Mock JY, Wang X, Martin AD, Tokatlian T, et al. Structure-function relationships of chimeric antigen receptors in acute T cell responses to antigen. Mol Immunol. 2020;126:56–64.
19. Mitaksov V, Truscott SM, Lybarger L, Connolly JM, Hansen TH, Fremont DH. Structural engineering of pMHC reagents for T cell vaccines and diagnostics. Chem Biol. 2007;14(8):909–22.
20. Burshtyn DN, Lam AS, Weston M, Gupta N, Warmerdam PAM, Long EO. Conserved residues amino-terminal of cytoplasmic tyrosines contribute to the SHP-1-mediated inhibitory function of killer cell Ig-like receptors. J Immunol. 1999;162(2):897–902.
21. Aarnoudse CA, Krüse M, Konopitzky R, Brouwenstijn N, Schrier PI. TCR reconstitution in Jurkat reporter cells facilitates the identification of novel tumor antigens by cDNA expression cloning. Int J Cancer. 2002;99(1):7–13.
22. Arlot S, Celisse A. A survey of cross-validation procedures for model selection. Statistics Surveys. 2010;4:40–79.
23. Zurowski D, Patel S, Hui D, Ka M, Hernandez C, Love AC, et al. High-throughput method to analyze the cytotoxicity of CAR-T cells in a 3D tumor spheroid model using image cytometry. SLAS Discov. 2023;28(3):65–72.
24. Le K, Tan C, Gupta S, Guhan T, Barkhordarian H, Lull J, et al. A novel mammalian cell line development platform utilizing nanofluidics and optoelectro positioning technology. Biotechnol Prog. 2018;34(6):1438–46.
25. Goodman DB, Azimi CS, Kearns K, Talbot A, Garakani K, Garcia J, et al. Pooled screening of CAR T cells identifies diverse immune signaling domains for next-generation immunotherapies. Sci Transl Med. 2022;14(670):eabm1463.
26. Gordon KS, Kyung T, Perez CR, Holec PV, Ramos A, Zhang AQ, et al. Screening for CD19-specific chimaeric antigen receptors with enhanced signalling via a barcoded library of intracellular domains. Nat Biomed Eng. 2022;6(7):855–66.
27. Castellanos-Rueda R, di Roberto RB, Bieberich F, Schlatter FS, Palianina D, Nguyen OTP, et al. speedingCARs: Accelerating the engineering of CAR T cells by signaling domain shuffling and single-cell sequencing. Nat Commun. 2022;13(1):6555.

SUPPORTING INFORMATION

Additional supporting information can be found online in the Supporting Information section at the end of this article.

How to cite this article: Martire S, Wang X, McElvain M, Suryawanshi V, Gill T, DiAndreth B, et al. High-throughput screen to identify and optimize NOT gate receptors for cell therapy. Cytometry. 2024. https://doi.org/10.1002/cyto.a.24893